

# CONSTRAINTS ON THE MINIMAL SUPERGRAVITY MODEL FROM NON-STANDARD VACUA

Howard Baer, Michal Brhlik and Diego Castaño

*Department of Physics, Florida State University, Tallahassee, FL 32306 USA*

(October 7, 2018)

## Abstract

We evaluate regions of parameter space in the minimal supergravity model where “unbounded from below” (UFB) or charge or color breaking minima (CCB) occur. Our analysis includes the most important terms from the 1-loop effective potential. We note a peculiar discontinuity of results depending on how renormalization group improvement is performed: One case leads to a UFB potential throughout the model parameter space, while the other typically agrees quite well with similar calculations performed using only the tree level potential. We compare our results with constraints from cosmology and naturalness and find a preferred region of parameter space which implies  $m_{\tilde{g}} \lesssim 725$  GeV,  $m_{\tilde{q}} \lesssim 650$  GeV,  $m_{\tilde{W}_1} \lesssim 225$  GeV and  $m_{\tilde{\ell}_R} \lesssim 220$  GeV. We discuss the consequences of our results for supersymmetry searches at various colliding beam facilities.

arXiv:hep-ph/9607465v1 29 Jul 1996

## I. INTRODUCTION

The Minimal Supersymmetric Standard Model (MSSM) is one of the leading candidate models [1] for physics beyond the Standard Model (SM). In this theory, one begins with the SM particles (but with two Higgs doublets to ultimately ensure anomaly cancellation); supersymmetrization then leads to partner particles for each SM particle which differ by spin- $\frac{1}{2}$ . Supersymmetry breaking is implemented by adding explicit soft supersymmetry breaking terms. This procedure leads to a particle physics model with  $\gtrsim 100$  free parameters, which ought to be valid at the weak scale.

To reduce the number of free parameters, one needs a theory of how the soft SUSY breaking terms arise, *i.e.*, how supersymmetry is broken. In the minimal supergravity model (SUGRA) [2], supersymmetry is spontaneously broken via a hidden sector field vacuum expectation value (VEV), and the SUSY breaking is communicated to the visible sector via gravitational interactions. For a flat Kähler metric and common gauge kinetic functions, this leads to a common scalar mass  $m_0$ , a common gaugino mass  $m_{1/2}$ , and common trilinear and bilinear terms  $A_0$  and  $B_0$  at some high scale  $M_{\text{GUT}} - M_{\text{Pl}}$ , where the former choice is usually taken due to apparent gauge coupling unification at  $\sim 2 \times 10^{16}$  GeV. The high scale mass terms and couplings are then linked to weak-scale values via renormalization group evolution. Electroweak symmetry breaking [3], which is hidden at high scales, is then induced by the large top-quark Yukawa coupling, which drives one of the Higgs field masses to a negative value. Minimization of the scalar potential allows one to effectively replace  $B$  by  $\tan \beta$  and express the magnitude (but not the sign) of the Higgsino mass  $\mu$  in terms of  $M_Z$ . The resulting parameter space of this model is thus usually given by the set  $(m_0, m_{1/2}, A_0, \tan \beta, \text{and } \text{sign}(\mu))$ .

Not all values of the above 4 + 1 dimensional parameter space of the minimal SUGRA model are allowed. For instance, the top and bottom Yukawa couplings are driven to infinity somewhere between  $M_Z$  and  $M_{\text{GUT}}$  for  $\tan \beta \lesssim 1.5$  and  $\gtrsim 50$  (depending on the value of  $m_t$ ) [4]. For other parameter choices, the lightest chargino or lightest slepton (or top squark) can be the lightest SUSY particle, which would violate limits on, for instance, heavy exotic nuclei. For yet other parameter choices, electroweak symmetry breaking leads to the wrong value of  $M_Z$ , so these parameter choices are ruled out. In addition, there are cosmological bounds from the relic density of neutralinos produced in the Big Bang [5]. Requiring the universe to be older than  $\sim 10$  billion years leads to only a subset of the parameter space being allowed, although this bound could be evaded by allowing for a small amount of R-parity violation. Finally, certain regions of parameter space are rejected by negative searches for sparticles at colliding beam experiments, such as those at LEP and the Fermilab Tevatron [6].

An additional constraint on minimal SUGRA parameters can be obtained by requiring that the global minimum of the scalar potential is indeed the minimum that leads to appropriate electroweak symmetry breaking. In the SM, there is only a single direction in the field space of the scalar potential, so appropriate electroweak symmetry breaking can be assured. For the MSSM, the plethora of new scalar fields which are introduced leads to many possible directions in field space where minima could develop which are deeper than the standard minimum. Thus, parameter choices which lead to deeper minima should be excluded as well, since they would lead to a universe with a non-standard vacuum.

Constraints along the preceding lines were developed in Refs. [7] in the early 1980's, using the renormalization group improved tree level effective potential. It was noted by Gamberini *et. al.* [8] that the renormalization group improved tree potential was subject to large variations due to uncertainty in the correct scale choice  $Q$  at which it was evaluated. Inclusion of 1-loop corrections served to ameliorate this condition. Recently, Casas, Lleyda, and Muñoz [9] have made a systematic survey of all possible dangerous directions in scalar field space that can potentially lead to minima deeper than the standard one. These have been categorized as field directions that are either unbounded from below (at tree level) (UFB) or that lead to charge or color-breaking (CCB) minima. For simplicity, their analysis uses the tree-level scalar potential but evaluated at an optimized mass scale where 1-loop corrections ought to be only a small effect. Working within the minimal SUGRA model, they considered models with  $B_0 = A_0 - m_0$  or  $B_0 = 2m_0$  and showed that significant regions of parameter space could be excluded via this method.

In the present work, one of our main goals is to delineate the parameter space regions where non-standard potential minima develop in such a manner as to facilitate comparisons with other constraints, including recently calculated results on the neutralino relic density [10] and parameter space regions favored by fine-tuning considerations [11]. In addition, expectations for supersymmetry at LEP2 [12], the Tevatron MI and TeV33 upgrades [13], the LHC [14], and NLC [15] have been calculated within the minimal SUGRA framework. We also compare the non-standard vacuum constraints with the various collider expectations and draw some conclusions. For instance, combining the non-standard vacuum constraints with the most favored parameter space regions from fine-tuning and cosmology suggests that the Fermilab TeV33 upgrade stands a high chance to discover SUSY via the  $\tilde{W}_1 \tilde{Z}_2 \rightarrow 3\ell$  signal!

In the present work, we also adopt a somewhat different calculational scheme from that employed in Ref. [9]. For all field directions considered, we implement renormalization group (RG) improvement to calculate the 1-loop effective potential. We find that the inclusion of the 1-loop correction has important consequences. The 1-loop correction almost always represents a significant contribution to the tree level potential. Nevertheless, our overall results agree very well with those of [9] for a “proper” choice in RG improvement scheme. For reference, we shall call this the “ $\alpha$ -case,” and it represents our main results. However, for other choices of RG improvement, we find that the 1-loop correction can be so dominant as to lead to unbounded from below (UFB) potentials everywhere in parameter space: We refer to this as the “ $\omega$ -case.” Because this is a multi-scale problem, it is not entirely clear how to proceed with RG improvement, and it is this ambiguity that leads to the two cases above. The validity of our results hinge on two main assumptions. The first concerns the adequacy of cutting the expansion at 1-loop. It is beyond the present analysis to ascertain the significance of the 2-loop contribution in any of the cases considered. However, because of the dependence of our results on the details of RG improvement, we believe that the 2-loop contribution may be important. Secondly, we have only included the contribution of the top-stop sector in our calculations of the 1-loop correction. It remains to be determined if the inclusion of the other fields will significantly affect the results.

We note briefly that the work of [16] and [17] advances the idea that we may indeed exist in a false vacuum and that the tunnelling rate from our present vacuum to a UFB or CCB vacuum might be small relative to the age of the universe. In this case, the following derived

constraints would not be meaningful. Such a philosophy must, however, be reconciled [18] with the fact that we live in a world in which the cosmological constant either vanishes or is extremely small. This is empirical, albeit indirect, evidence for some mechanism which seeks to enforce the principle that “the cosmological constant of the true vacuum is zero.” It is difficult to conceive of circumstances where we could tenably entertain both the idea that we are living in a false vacuum and the idea that the smallness of the cosmological constant has a natural solution, since this would require a principle which would set the cosmological constant to zero in a false, broken vacuum while simultaneously leaving the true, broken vacuum with a large negative cosmological constant.

The organization of the paper is as follows. In Section II, we review the MSSM scalar potential and give a brief summary of the UFB and CCB directions delineated in Ref. [9]. In Section III, we present our calculational procedure and in Sec. IV present results of our scans over SUGRA parameter space. In Section V we give a brief summary of our results. Detailed formulae for the effective potential in various UFB and CCB directions are included in Appendix A, while some computationally useful formulae for evaluating the effective potential in the limit of large VEVs is presented in Appendix B.

## II. DANGEROUS DIRECTIONS IN FIELD SPACE

The scalar potential of the MSSM can be written as

$$V = V_F + V_D + V_{\text{soft}} , \quad (2.1)$$

where

$$\begin{aligned} V_F &= \sum_{\alpha} \left| \frac{\partial W}{\partial \phi_{\alpha}} \right|^2 \\ &= \left| \sum_i \bar{u}_i y_{u_i} Q_i + \mu \Phi_d \right|^2 + \left| \sum_i (y_{d_i} \bar{d}_i Q_i + y_{e_i} \bar{e}_i L_i) + \mu \Phi_u \right|^2 \\ &+ \sum_i |y_{u_i} \Phi_u Q_i|^2 + \sum_i |y_{d_i} \Phi_d Q_i|^2 + \sum_i |y_{e_i} \Phi_d L_i|^2 \\ &+ \sum_i |y_{u_i} \bar{u}_i \Phi_u + y_{d_i} \bar{d}_i \Phi_d|^2 + \sum_i |y_{e_i} \bar{e}_i \Phi_d|^2 , \end{aligned} \quad (2.2)$$

$$\begin{aligned} V_D &= \frac{1}{2} \sum_a g_a^2 (\sum_{\alpha} \phi_{\alpha}^{\dagger} T^a \phi_{\alpha})^2 \\ &= \frac{g'^2}{2} \left[ \sum_i \left( \frac{1}{6} |Q_i|^2 - \frac{2}{3} |\bar{u}_i|^2 + \frac{1}{3} |\bar{d}_i|^2 - \frac{1}{2} |L_i|^2 + |\bar{e}_i|^2 \right) + \frac{1}{2} |\Phi_u|^2 - \frac{1}{2} |\Phi_d|^2 \right]^2 \\ &+ \frac{g_2^2}{8} \left[ \sum_i (Q_i^{\dagger} \vec{\tau} Q_i + L_i^{\dagger} \vec{\tau} L_i) + \Phi_u^{\dagger} \vec{\tau} \Phi_u + \Phi_d^{\dagger} \vec{\tau} \Phi_d \right]^2 \\ &+ \frac{g_3^2}{8} \left[ \sum_i (Q_i^{\dagger} \vec{\lambda} Q_i - \bar{u}_i^{\dagger} \vec{\lambda}^* \bar{u}_i - \bar{d}_i^{\dagger} \vec{\lambda}^* \bar{d}_i) \right]^2 , \end{aligned} \quad (2.3)$$

where  $\vec{\tau} = (\tau_1, \tau_2, \tau_3)$  are the  $SU(2)$  Pauli matrices, and  $\vec{\lambda} = (\lambda_1, \dots, \lambda_8)$  are the Gell-Mann  $SU(3)$  matrices.

$$\begin{aligned}
V_{\text{soft}} &= \sum_{\alpha} m_{\phi_{\alpha}}^2 |\phi_{\alpha}|^2 + (B\mu\Phi_u\Phi_d + c.c.) \\
&+ \sum_i \left( A_{u_i} y_{u_i} \bar{u}_i \Phi_u Q_i + A_{d_i} y_{d_i} \bar{d}_i \Phi_d Q_i + A_{e_i} y_{e_i} \bar{e}_i \Phi_d L_i + c.c. \right) ,
\end{aligned} \tag{2.4}$$

and the superpotential  $W$  is

$$W = \sum_i \left( y_{u_i} \bar{u}_i \Phi_u Q_i + y_{d_i} \bar{d}_i \Phi_d Q_i + y_{e_i} \bar{e}_i \Phi_d L_i \right) + \mu \Phi_u \Phi_d . \tag{2.5}$$

In the above,  $\phi_{\alpha}$  runs over the scalar components of the chiral superfields, and  $a, i$  are gauge group and generation indices, respectively.  $Q_i$  ( $L_i$ ) are the scalar partners of the quark (lepton)  $SU(2)_L$  doublets, and  $\bar{u}_i, \bar{d}_i,$  and  $\bar{e}_i$  are the scalar partners of the  $SU(2)_L$  singlets.  $\Phi_u$  and  $\Phi_d$  are the two Higgs doublets. When all the above summations are performed, one is left with a very lengthy expression for the scalar potential. In the following, usually only a small number of scalar fields develop VEVs, so only a subset of the many terms of the scalar potential are relevant.

For the usual breaking of electroweak symmetry in the MSSM, only  $\Phi_u$  and  $\Phi_d$  develop VEVs, so that the relevant part of the above potential is just

$$\begin{aligned}
V_0 &= m_1^2 |\Phi_d|^2 + m_2^2 |\Phi_u|^2 + m_3^2 (\Phi_u \Phi_d + h.c.) \\
&+ \frac{g'^2}{8} (\Phi_u^{\dagger} \Phi_u - \Phi_d^{\dagger} \Phi_d)^2 + \frac{g_2^2}{8} (\Phi_u^{\dagger} \vec{\tau} \Phi_u + \Phi_d^{\dagger} \vec{\tau} \Phi_d)^2,
\end{aligned} \tag{2.6}$$

where the masses appearing above are defined as

$$m_1^2 = m_{\Phi_d}^2 + \mu^2 , \tag{2.7}$$

$$m_2^2 = m_{\Phi_u}^2 + \mu^2 , \tag{2.8}$$

$$m_3^2 = B\mu . \tag{2.9}$$

The 1-loop contribution to the scalar potential is given by

$$\begin{aligned}
\Delta V_1(Q) &= \frac{1}{64\pi^2} \text{Str} \left\{ \mathcal{M}^4 \left( \ln \frac{\mathcal{M}^2}{Q^2} - \frac{3}{2} \right) \right\} \\
&= \frac{1}{64\pi^2} \sum_i (-1)^{2s_i} (2s_i + 1) m_i^4 \left( \ln \frac{m_i^2}{Q^2} - \frac{3}{2} \right) ,
\end{aligned} \tag{2.10}$$

where  $\mathcal{M}^2$  is the field dependent squared mass matrix of the model, and  $m_i$  is the mass of the  $i^{\text{th}}$  particle of spin  $s_i$ . In the 1-loop correction, we shall always include only the contribution from the top-stop sector, this being generally the most significant.

Minimization, at a scale  $Q$  usually taken to be  $M_Z$ , yields two conditions on the parameters

$$\frac{1}{2} m_Z^2 = \frac{\bar{m}_1^2 - \bar{m}_2^2 \tan^2 \beta}{\tan^2 \beta - 1} , \tag{2.11}$$

where  $m_Z^2 = \hat{g}^2 v^2 = (g'^2 + g_2^2) v^2 / 2$ ,  $v^2 = v_u^2 + v_d^2$ , and

$$B\mu = \frac{1}{2} (\bar{m}_1^2 + \bar{m}_2^2) \sin 2\beta , \tag{2.12}$$

with  $\tan \beta = v_u/v_d$ , and where the barred masses are the 1-loop analogs of (2.7-2.8). At this point, the minimum of the tree-potential is

$$V_{\min} = -\frac{1}{4\hat{g}^2} \left[ (m_1^2 - m_2^2) + (m_1^2 + m_2^2) \cos 2\beta \right]^2 . \quad (2.13)$$

The field dependent top and stop masses are given by

$$\begin{aligned} m_t &= y_t v_u , \\ m_{t_{1,2}}^2 &= m_t^2 + \frac{1}{2}(m_{Q_3}^2 + m_{\bar{u}_3}^2) + \frac{1}{4}m_Z^2 \cos 2\beta \\ &\pm \sqrt{\left[ \frac{1}{2}(m_{Q_3}^2 - m_{\bar{u}_3}^2) + \frac{1}{12}(8m_W^2 - 5m_Z^2) \cos 2\beta \right]^2 + m_t^2 (A_t + \mu \cot \beta)^2} , \end{aligned} \quad (2.14)$$

where  $m_W^2 = g_2^2 v^2/2$ . We will compare the value of the potential at the MSSM minimum with the value at the minimum for other field configurations and use this to reject MSSM scenarios with false vacua.

The dangerous directions in field space have been categorized in Ref. [9] as various UFB and CCB directions. For the UFB directions, the trilinear scalar terms are unimportant. To find the deepest directions in field space, one searches for directions where the D-terms of Eq. (2.3) will be small or vanishing. The various UFB directions are characterized as

- **UFB-1:** Here, only the fields  $\Phi_u$  and  $\Phi_d$  obtain VEVs, with  $\langle \Phi_u \rangle = \langle \Phi_d \rangle$  in order to cancel D-terms in 2.6.
- **UFB-2:** In addition to the VEVs  $\langle \Phi_u \rangle$  and  $\langle \Phi_d \rangle$ , one has a VEV for the 3rd generation slepton field in the  $\nu$  direction:  $\langle L_3 \rangle_\nu$ . The VEVs are related as in Eq. (A.3).
- **UFB-3a:** In this case, the relevant VEVs are  $\langle \Phi_u \rangle$ ,  $\langle L_3 \rangle_e^2 = \langle \bar{e}_3 \rangle^2$ , and  $\langle L_2 \rangle_\nu$ . This direction reputedly leads to the most stringent bounds on parameter space. The VEVs are related as in Eq. (A.10).
- **UFB-3b:** This case is similar to UFB-3a, but instead of the first two slepton fields,  $\langle Q_3 \rangle_d^2 = \langle \bar{d}_3 \rangle^2$  develop VEVs. The VEVs are related as in Eq. (A.16).

The various CCB directions each involve a particular trilinear coupling. For each trilinear coupling, there are two relevant directions: CCB(a) (equivalent to Casas *et. al.* CCB-1), and CCB(b) (which combines the CCB-2 and CCB-3 cases of Casas *et. al.*). The CCB(a) direction is not relevant for the top trilinear term. Summing over the various trilinear terms and CCB directions can yield at least 17 possible directions (some other possible directions lead to essentially the same constraints). For illustration, we investigated the following cases, which include cases with the largest and smallest Yukawa couplings.

- **CCB(a)-UP:** The relevant VEVs are  $\langle \Phi_u \rangle$ ,  $\langle Q_1 \rangle_u$ ,  $\langle \bar{u}_1 \rangle$ ,  $\langle Q_3 \rangle_d^2 = \langle \bar{d}_3 \rangle^2$ , and  $\langle L_3 \rangle_\nu$ , with  $\langle \Phi_d \rangle = 0$ . The VEVs are related as in Eq. (A.22).
- **CCB(b)-UP:** The relevant VEVs are  $\langle \Phi_u \rangle$ ,  $\langle \Phi_d \rangle$ ,  $\langle Q_1 \rangle_u$ ,  $\langle \bar{u}_1 \rangle$ , and  $\langle L_3 \rangle_\nu$ . The VEVs are related as in Eq. (A.28).

- **CCB(b)-TOP:** The relevant VEVs are  $\langle \Phi_u \rangle$ ,  $\langle \Phi_d \rangle$ ,  $\langle Q_3 \rangle_u$ ,  $\langle \bar{u}_3 \rangle$ , and  $\langle L_3 \rangle_\nu$ . The VEVs are related as in Eq. (A.42).
- **CCB(a)-ELECTRON:** The relevant VEVs are  $\langle \Phi_d \rangle$ ,  $\langle L_1 \rangle_e$ ,  $\langle \bar{e}_1 \rangle$ , and  $\langle Q_3 \rangle_u^2 = \langle \bar{u}_3 \rangle^2$ , with  $\langle \Phi_u \rangle = 0$ . The VEVs are related as in Eq. (A.58).
- **CCB(b)-ELECTRON:** Lastly, the relevant VEVs are  $\langle \Phi_d \rangle$ ,  $\langle \Phi_u \rangle$ ,  $\langle L_1 \rangle_e$ , and  $\langle \bar{e}_1 \rangle$ . The VEVs are related as in Eq. (A.63).

### III. CALCULATIONAL DETAILS

The standard procedure for studying the MSSM has been, as summarized above, to fix the parameters  $B_0$  and  $\mu_0$  in order to achieve symmetry breaking as dictated by (2.7) and (2.8) with  $v = 174$  GeV. Furthermore, the choice in minimization scale being in the  $M_Z$  range is dictated by the desired vacuum expectation value and is validated by the use of the 1-loop correction. Unfortunately, this method does not lend itself to the present task, since *a priori* the minimum of the potential in a given configuration is unknown. The task is complicated since we must be able to probe the potential for significantly different field values.

In order to validate the use of the 1-loop effective potential, one must ensure that not only the couplings be perturbative but that the logarithms be small as well. This is the process of RG improvement [19]. In problems with only one mass scale, RG improvement is straightforward. The logarithm appearing in the 1-loop correction can be made small, indeed to vanish, for any choice in field value by an appropriate choice in renormalization scale  $Q$ . This procedure yields the  $Q$ -independent, 1-loop RG improved potential. For the cases in which we are interested, there are several mass scales. Since in general no scale exists that simultaneously makes all the logarithms vanish, we settle for the scale at which the logarithms are simultaneously, optimally small. In this way, we construct the 1-loop effective potential. Note that in such cases the 1-loop correction does not vanish and indeed may represent a significant contribution to the tree level part. In our subsequent results, we always include the 1-loop correction in our evaluation of the effective potential. Figure 1 demonstrates the significance of the 1-loop correction for a representative case with  $A_0 = 0$ ,  $m_0 = 100$  GeV,  $m_{1/2} = 200$  GeV,  $\tan\beta(M_Z) = 2$ , and  $\mu < 0$ . In this example, we have employed the  $\alpha$ -scheme (see below) for RG improvement. From Fig. 1b we see that the difference between the value of the tree potential at the minimum and the 1-loop effective potential in the UFB-3(a) direction is almost a factor of four. There is also an effect in the standard MSSM direction as seen in Fig. 1a. This particular point in parameter space is ruled out since  $V_{\min}^{\text{UFB-3(a)}} < V_{\min}^{\text{MSSM}}$ . We implement the RG improvement procedure as follows: (1) At each RG scale  $Q$  find the field value  $\phi$  that minimizes the function

$$f(\phi, Q) = \sum_i \left[ \log \left\{ m_i^2(\phi, Q) / Q^2 \right\} - \chi \right]^2, \quad (3.1)$$

(2) store this value and the corresponding  $V_1(\phi, Q)$ . This results in the function  $(\phi, V_{\text{RGI}}(\phi))$  whose minimum can then be calculated.

Given the standard numerical procedure involved in RG studies, in which Runge-Kutta routines are used to integrate over  $Q$ , the above procedure of finding the optimal  $\phi$  at each

scale  $Q$  is the most efficient, since we construct the RG improved potential simultaneously as we evolve the RG parameters of the MSSM. Also, we note that including  $m_i^4$  coefficients in  $f(\phi, Q)$  (as they appear in  $\Delta V_1$ ) leads to pathological results. Namely, at all scales  $Q$ , the  $f$ -minimizing field value tends to zero. This is a pathology of the method we are employing. Had we instead fixed  $\phi$  and found the  $f$ -minimizing value of  $Q$ , this problem would not be present. Because of the ambiguities in RG improvement in multi-scale problems, we examined several prescriptions for constructing the effective potential. Eq. (2.9) with  $\chi = 3/2$  led to the  $\alpha$ -case. We also tried  $\chi = 0$ . We used the functional form  $f = \ln^2\{m^2/Q^2\}$ , and tried the top and stop masses as possible choices for  $m$ . All of these choices led to the  $\omega$ -case. In this case, the potentials along the UFB-3(b) and CCB(a)-UP directions were unbounded from below everywhere in parameter space. Although this result is interesting, we believe that 2-loop leading logarithms may remedy this curious situation. Therefore we discount these results for the moment. Along all other directions considered, the  $\omega$ -results were similar to the  $\alpha$ -results as one expects. Figure 2 displays results in the  $\omega$ -case similar to Fig. 1. Comparing Figs. 1 and 2, the 1-loop effective potentials are essentially identical for the MSSM direction. And although the UFB-3(a) potentials are clearly different, the  $\omega$  potential in this direction remains well-behaved. Figure 3 displays the logarithm of the VEV versus  $\chi$  in two vacuum directions. In the UFB-3(a) direction, there is some minor change in the VEV but not very significant as  $\chi$  varies from the  $\alpha$  to  $\omega$  value. In contrast, the VEV suffers a drastic, discontinuous jump at around  $\chi = 1$  in the CCB(a)-UP direction. This same discontinuity occurs in the UFB-3(b) case.

From Fig. 3, we see that altering  $\chi$  (which effectively changes our  $Q$  choice) changes our results dramatically in the CCB(a)-UP and UFB-3(b) directions. These two directions are special in that their 1-loop contributions are dominant in the large VEV domain. This comes in particular from contributions to the stop masses by the  $y_{b,t}^2 d^2$  terms (see (A.19-20,25-26)); bear in mind that the quadratic (or  $G_{\pm}$ ) contributions in  $x$  are always small or zero. For these cases, in the large VEV domain, the 1-loop correction,  $\Delta V_1$ , is obviously unstable against  $Q$ . For the case depicted in Fig. 3, we have verified that  $V_1(Q, \Phi_u = 10^{16} \text{ GeV})$  has a large, negative slope and changes sign at  $Q \approx 4 \times 10^{15} \text{ GeV}$ , leading to a potential which is very unstable against variations in scale choice. We assume this instability is due to a need to include higher terms in the effective potential for these cases.

It is interesting to note that the standard procedure for computing the MSSM minimum gives results that differ, sometimes greatly, from the above RG improved procedure. We find that the 1-loop correction to the MSSM potential does a poor job of stabilizing the potential against  $Q$  near  $M_Z$ . This was alluded to in [20]. The result is surprising given the conventional lore that the 1-loop correction stabilizes the potential in the electroweak range. A more detailed study of this issue is in progress. In Fig. 4, we demonstrate the problem by displaying the  $Q$  evolution of the VEV using two different methods in the case  $A_0 = 0$ ,  $m_0 = m_{1/2} = 100 \text{ GeV}$ ,  $\tan\beta(M_Z) = 2$ , and  $\mu < 0$ . The solid line represents the evolution as dictated by the RG gamma functions of the Higgs fields (see [21]). The dashed line represents the tracking of the minimum of the 1-loop effective potential. Here we have included the contributions from *all* particles in  $\Delta V_1$ .

For all cases, we have explored the dangerous directions delineated in Ref. [9]; these directions were obtained using only the tree level potential. A better procedure would involve optimization of the full 1-loop effective potential. This may in principle lead to even more

precipitous directions. However, since this procedure leads to very unwieldy expressions, we have opted to explore the tree-level-derived directions in field space, although in these directions we make comparisons using the 1-loop corrected scalar potential.

We emphasize the importance of using the 1-loop correction to the scalar potential, since its inclusion can alter the depth of the minimum significantly as was evident in Fig. 1*b*. Furthermore, the startling results of the  $\omega$ -case were a consequence of using the 1-loop correction to compute the potential. Had the 1-loop correction been ignored, all choices of RG improvement we tried would have led to results similar to [9]. Figure 5*a* shows the potential along the CCB(a)-UP direction (in the case  $A_0 = 0$ ,  $m_0 = 100$ ,  $m_{1/2} = 200$ ,  $\tan\beta(M_Z) = 2$ , and  $\mu < 0$ ) using only the tree level potential. This point would have been excluded by the CCB(a)-UP constraint since  $V_{\min}^{\text{CCB(a)-UP}} < V_{\min}^{\text{MSSM}}$ . However, including the 1-loop correction in this case leads to the potential displayed in Fig. 5*b*. It appears unbounded from below as last seen at field values nearing the Planck scale in the  $\omega$ -case thus also ruling out this point. However, in the same figure, the  $\alpha$ -case 1-loop effective potential is not unbounded from below and indeed does not rule out this point (in this direction).

#### IV. RESULTS

Using the procedures outlined in Sec. III and Appendices A and B, we explored regions of minimal SUGRA parameter space for minima deeper than the standard MSSM one. Our initial scans took place in the  $m_0$  vs.  $m_{1/2}$  plane, to facilitate comparison with recent results on fine-tuning, cosmology and present and future collider searches. We fix  $\tan\beta(M_Z)$  to be 2 or 10, take  $A_0 = 0$  and  $m_t = 170$  GeV. Our search was performed in the ranges  $0 \leq m_0, m_{1/2} \leq 500$  GeV and the grid was scanned with 25 GeV resolution. Figures 6*a-d* display the regions where non-standard global minima were discovered. Of all the directions scanned for these plots, non-standard vacua were found only in the UFB-3a direction. In Fig. 6, we have encoded information about the magnitude of the VEV in the plotting symbol. Using  $\eta = \log_{10}\{v/v_{\text{MSSM}}\}$ , the squares represent  $2 < \eta < 3$ , the crosses  $3 < \eta < 4$ , and the x's  $4 < \eta < 5$ . The most dangerous regions are those populated by squares: For these points the “distance” between the standard and non-standard minima is smallest, which would admit the largest rate for tunnelling between them. Performing this scan using the exact prescription of Ref. [9] leads to nearly identical excluded regions.

We see from Fig. 6 that for all four frames, the region of low  $m_0$  becomes excluded. As noted in Ref. [9], this rules out the so-called “no-scale” models which require  $m_0 = 0$ . In addition, in string models where supersymmetry is broken in the dilaton sector, one is led to GUT or string scale soft-terms related by  $m_{1/2} = -A_0 = \sqrt{3}m_0$  [22,23]. For this precise choice of soft-term boundary conditions, much of the parameter space is excluded by non-standard minima. We further note that the excluded region rules out much of the SUGRA parameter space associated with light sleptons. In particular, taken literally, our results exclude regions where such decays as  $\tilde{Z}_2 \rightarrow \tilde{\ell}_L \bar{\ell}$  and  $\tilde{Z}_2 \rightarrow \tilde{\nu} \bar{\nu}$  take place.

Although Fig. 6 is plotted for  $A_0 = 0$ , a similar excluded region results for other choices of the  $A_0$  parameter. This is shown in Fig. 7, where we plot regions excluded in the  $m_0$  vs.  $A_0$  plane, for the same values of  $\tan\beta$  and  $\mu$ , but for  $m_{1/2}$  fixed at 200 GeV. The vacuum constraints exist for all  $A_0$  values, but are smallest for  $A_0 \sim 300$  GeV.

In Fig. 8, we display a combined plot of Fig. 6 with superposed dark matter [10] and fine tuning [11] contours. The regions to the right of the solid line contours are cosmologically excluded because they predict a relic density  $\Omega h^2 > 1$ ; this corresponds to a lifetime of the universe of less than 10 billion years. Cosmological models which take into account COBE data, nucleosynthesis, and large-scale structure formation prefer an inflationary cosmology, with a matter content of the universe comprising 60% cold dark matter (*e.g.*, neutralinos), 30% hot dark matter (*e.g.*, neutrinos), and 10% baryonic matter. In this case, the preferred relic density of neutralinos should be  $.15 < \Omega h^2 < .4$ , *i.e.*, the region between the dot-dashed contours. In addition, Fig. 8 contains two naturalness contours with varying degrees of acceptability:  $\tilde{\gamma}_2 = 5$  and 10 [11]. The more encompassing contour is a conservative estimate of a reasonable “tolerance limit” for weak scale supersymmetry. We see that the constraint from false vacua overlaps considerably with the preferred regions from cosmology and fine-tuning, leaving only a small preferred region of parameter space around  $m_0 \sim 100 - 200$ , and  $m_{1/2} \sim 100 - 250$  in each frame. We note that the resulting preferred region of parameter space requires  $m_{\tilde{g}}, m_{\tilde{q}}, m_{\tilde{W}_1}, m_{\tilde{\ell}_R} \lesssim 650, 600, 220$  and  $175$  GeV, respectively, for  $\tan \beta = 2$ , and  $m_{\tilde{g}}, m_{\tilde{q}}, m_{\tilde{W}_1}, m_{\tilde{\ell}_R} \lesssim 725, 650, 225$  and  $220$  GeV for  $\tan \beta = 10$ . The only exception to these bounds is if the neutralino is poised near the peak of an *s*-channel pole in its annihilation cross section. These regions correspond to the narrow horizontal corridors in the relic density contours.

Recently, the reach of the Fermilab Main Injector and TeV33 have been calculated in the same parameter space frames [13]. By comparing the results of Ref. [13] with the preferred parameter space discussed above, we see that the TeV33 option covers most of the preferred region from Fig. 8*a* via the clean trilepton signal from  $\tilde{W}_1 \tilde{Z}_2 \rightarrow 3\ell$ , the exception being the region with  $m_{1/2} \gtrsim 180$  GeV, where the spoiler decay mode  $\tilde{Z}_2 \rightarrow \tilde{Z}_1 h$  turns on. For Fig. 8*b*, TeV33 will cover the *entire* preferred region via clean trileptons. For the large  $\tan \beta = 10$  cases of Figs. 8*c* and *d*, the TeV33 upgrade can see most, but not all, of the preferred parameter space regions. The reach of the Tevatron Main Injector is significantly less than TeV33 for these preferred regions of parameter space. The CERN LHC collider can of course probe all the preferred regions of parameter space. In fact, event rates will be enormous for various multi-lepton + multi-jet +  $\cancel{E}_T$  channels, which should facilitate precision measurements of parameters [14]. In particular, sleptons have mass less than 250 GeV in these regions, and so ought to be visible at the LHC. Finally, we note that both the light chargino and right-selectron have mass less than 250 GeV in the preferred regions, so that both of these sparticles would be accessible to Next Linear Collider (NLC) experiments operating at  $\sqrt{s} = 500$  GeV [15].

## V. CONCLUSION

The minimal SUGRA model provides a well-motivated and phenomenologically viable picture of how weak scale supersymmetry might occur. The 4+1 dimensional parameter space can be constrained in numerous ways as discussed in the introduction. To constrain the model further, we have pursued the idea that parameter values that lead to global minima in non-standard directions, such as those with charge or color breaking, should be excluded from consideration. There are cosmological issues pertaining to tunnelling that we have knowingly ignored. Nevertheless, with this limitation noted, we searched for the

preferred regions of parameter space. We analyzed the potentials carefully employing the 1-loop correction including the contributions of the top and stops in the calculation. In generating the potential we found that the 1-loop correction can significantly alter results based only on the tree approximation.

Because of the various scales present in the MSSM, renormalization group improvement has ambiguities associated with it. We tried several procedures but were ultimately led to two distinct results that we refer to as the  $\alpha$ - and  $\omega$ -cases. In the  $\omega$ -case, to our surprise, the entire parameter space of the model suffers from global minima along non-standard directions (namely the UFB-3(b) and CCB(a)-UP directions). Since the 2-loop correction may be significant, given the large value of the top mass, the results in the  $\omega$ -case, while intriguing, must be taken *cum grano salis*.

In the  $\alpha$ -case, we are still left with a very restricted region of parameter space after imposing in addition dark matter and naturalness constraints. Most of this region should be accessible to the Fermilab TeV33 collider upgrade via the clean trilepton channel. This parameter space region should be entirely explorable at the LHC, and should yield a rich harvest of multilepton signals for supersymmetry which ought to allow for precision determination of underlying parameters. In addition, both charginos and sleptons ought to be accessible to NLC experiments operating at just  $\sqrt{s} = 500$  GeV, so that the underlying assumptions of the minimal SUGRA model can be well-tested.

#### ACKNOWLEDGMENTS

We thank Xerxes Tata and Greg Anderson for discussions. This research was supported in part by the U. S. Department of Energy under grant number DE-FG-05-87ER40319.

## APPENDIX A:

In this appendix, the cases from [9] that are considered in our investigation are reviewed. Also, formulas for the top/stops are displayed in each case and for the bottom/sbottoms in the last case.

• **UFB-1:** In the UFB-1 case, the only fields acquiring non-zero VEVs are  $\langle \Phi_u \rangle = \langle \Phi_d \rangle = x$ . The resulting tree level potential in this direction is

$$V = (m_1^2 + m_2^2 - 2|m_3^2|) x^2 , \quad (\text{A.1})$$

where  $m_1^2 = m_{\Phi_d}^2 + \mu^2$ ,  $m_2^2 = m_{\Phi_u}^2 + \mu^2$ , and  $m_3^2 = B\mu$ . The top mass is  $M_t = y_t x$ , and the stop mass matrix entries are

$$\begin{aligned} \tilde{M}_{LL}^2 &= m_{Q_3}^2 + y_t^2 x^2 , \\ \tilde{M}_{RR}^2 &= m_{u_3}^2 + y_t^2 x^2 , \\ \tilde{M}_{LR}^2 &= y_t (\mu - A_t) x . \end{aligned} \quad (\text{A.2})$$

• **UFB-2:** In the UFB-2 case, an additional slepton field is included to help control the D-terms. The shifted fields are therefore

$$\begin{aligned} \langle \Phi_u \rangle &= x , \\ \langle \Phi_d \rangle &= \gamma x , \\ \langle L_3 \rangle_\nu &= \gamma_L x . \end{aligned} \quad (\text{A.3})$$

The  $\nu$  subscript represents the SU(2) direction that has acquired the VEV. The scalar potential in this case is

$$V = \gamma^2 m_1^2 x^2 + m_2^2 x^2 - 2\gamma|m_3^2|x^2 + \gamma_L^2 m_{L_3}^2 x^2 + \frac{1}{4} \hat{g}^2 [1 - \gamma^2 - \gamma_L^2]^2 x^4 . \quad (\text{A.4})$$

Minimization with respect to  $\gamma$  and  $\gamma_L^2$  gives

$$\gamma = \frac{|m_3^2|}{m_1^2 - m_{L_3}^2} , \quad (\text{A.5})$$

$$\gamma_L^2 = 1 - \gamma^2 - \frac{2m_{L_3}^2}{\hat{g}^2 x^2} . \quad (\text{A.6})$$

If  $\gamma_L^2 < 0$ , then  $\gamma_L^2 = 0$ , and we recover the UFB-1 direction. In this case, the top mass is  $M_t = y_t x$ , and the stop mass matrix entries are

$$\tilde{M}_{LL}^2 = m_{Q_3}^2 + y_t^2 x^2 + \left( \frac{1}{12} g'^2 - \frac{1}{4} g^2 \right) [1 - \gamma^2 - \gamma_L^2] x^2 , \quad (\text{A.7})$$

$$\tilde{M}_{RR}^2 = m_{u_3}^2 + y_t^2 x^2 - \frac{1}{3} g'^2 [1 - \gamma^2 - \gamma_L^2] x^2 , \quad (\text{A.8})$$

$$\tilde{M}_{LR}^2 = y_t (\mu\gamma - A_t) x . \quad (\text{A.9})$$

• **UFB-3(a):** In the UFB-3(a) case, the shifted fields are

$$\begin{aligned}
\langle \Phi_u \rangle &= x , \\
\langle \Phi_d \rangle &= 0 , \\
\langle L_3 \rangle_e^2 &= \langle \bar{e}_3 \rangle^2 = \ell^2 = \left| \frac{\mu x}{y_\tau} \right| , \\
\langle L_2 \rangle_\nu &= \gamma_L x .
\end{aligned} \tag{A.10}$$

The VEVs of the  $(e_3, \bar{e}_3)$  sleptons are fixed by imposing  $\Phi_d$  F-term cancellation in the potential. The scalar potential for this case is

$$V = m_{\Phi_u}^2 x^2 + (m_{L_3}^2 + m_{\bar{e}_3}^2) \ell^2 + \gamma_L^2 m_{L_2}^2 x^2 + \frac{1}{4} \hat{g}^2 [x^2 + \ell^2 - \gamma_L^2 x^2]^2 . \tag{A.11}$$

Minimization with respect to  $\gamma_L^2$  gives

$$\gamma_L^2 = 1 + \left| \frac{\mu}{y_\tau x} \right| - \frac{2m_{L_2}^2}{\hat{g}^2 x^2} . \tag{A.12}$$

If  $\gamma_L^2 < 0$ , then  $\gamma_L^2 = 0$ . In this case the top mass is  $M_t = y_t x$ , and the stop mass matrix entries are

$$\tilde{M}_{LL}^2 = m_{Q_3}^2 + y_t^2 x^2 + \left( \frac{1}{12} g'^2 - \frac{1}{4} g_2^2 \right) [x^2 + \ell^2 - \gamma_L^2 x^2] , \tag{A.13}$$

$$\tilde{M}_{RR}^2 = m_{\bar{u}_3}^2 + y_t^2 x^2 - \frac{1}{3} g'^2 [x^2 + \ell^2 - \gamma_L^2 x^2] , \tag{A.14}$$

$$\tilde{M}_{LR}^2 = -A_t y_t x . \tag{A.15}$$

• **UFB-3(b):** In the UFB-3(b) case, the shifted fields are

$$\begin{aligned}
\langle \Phi_u \rangle &= x , \\
\langle \Phi_d \rangle &= 0 , \\
\langle Q_3 \rangle_d^2 &= \langle \bar{d}_3 \rangle^2 = d^2 = \left| \frac{\mu x}{y_b} \right| , \\
\langle L_3 \rangle_\nu &= \gamma_L x .
\end{aligned} \tag{A.16}$$

The VEVs of the  $(d_3, \bar{d}_3)$  squarks are fixed by imposing  $\Phi_d$  F-term cancellation in the potential. The scalar potential appears as

$$V = m_{\Phi_u}^2 x^2 + (m_{Q_3}^2 + m_{\bar{d}_3}^2) d^2 + \gamma_L^2 m_{L_3}^2 x^2 + \frac{1}{4} \hat{g}^2 [x^2 + d^2 - \gamma_L^2 x^2]^2 . \tag{A.17}$$

Minimization with respect to  $\gamma_L^2$  gives

$$\gamma_L^2 = 1 + \left| \frac{\mu}{y_b x} \right| - \frac{2m_{L_3}^2}{\hat{g}^2 x^2} . \tag{A.18}$$

If  $\gamma_L^2 < 0$ , then  $\gamma_L^2 = 0$ . In this case the top mass is  $M_t = y_t x$ , and the stop mass matrix entries are

$$\tilde{M}_{LL}^2 = m_{Q_3}^2 + y_t^2 x^2 + y_b^2 d^2 + \frac{1}{12}g'^2 [x^2 + d^2 - \gamma_L^2 x^2] - \frac{1}{4}g_2^2 [x^2 - d^2 - \gamma_L^2 x^2] , \quad (\text{A.19})$$

$$\tilde{M}_{RR}^2 = m_{\bar{u}_3}^2 + y_t^2 x^2 + y_t^2 d^2 - \frac{1}{3}g'^2 [x^2 + d^2 - \gamma_L^2 x^2] , \quad (\text{A.20})$$

$$\tilde{M}_{LR}^2 = -A_t y_t x . \quad (\text{A.21})$$

• **CCB(a)-UP:** In the CCB(a) case for the up-trilinear, the shifted fields are

$$\begin{aligned} \langle \Phi_u \rangle &= x , \\ \langle \Phi_d \rangle &= 0 , \\ \langle Q_1 \rangle_u &= \alpha x , \\ \langle \bar{u}_1 \rangle &= \beta x , \\ \langle Q_3 \rangle_d^2 &= \langle \bar{d}_3 \rangle^2 = d^2 = \left| \frac{\mu x}{y_b} \right| , \\ \langle L_3 \rangle_\nu &= \gamma_L x . \end{aligned} \quad (\text{A.22})$$

SU(3) D-flatness implies  $\beta^2 = \alpha^2$ . Also, U(1) and SU(2) D-flatness imply  $1 - \alpha^2 - \gamma_L^2 = 0$ . Consequently, the scalar potential appears as

$$V = y_u^2 (2 + \alpha^2) \alpha^2 x^4 - 2T_1 \alpha^2 x^2 + (M^2 \alpha^2 + m_{\Phi_u}^2 + m_\ell^2) x^2 , \quad (\text{A.23})$$

where  $T_1 = |A_u y_u x|$ ,  $M^2 = m_{Q_3}^2 + m_{\bar{u}_3}^2 - m_\ell^2$ , and  $m_\ell^2 = m_{L_3}^2$ . Minimization with respect to  $\alpha^2$  yields

$$\alpha^2 = \frac{T_1 - M^2/2 - y_u^2 x^2}{y_u^2 x^2} . \quad (\text{A.24})$$

If  $\alpha^2 < 0$ , then  $\alpha^2 = 0$  and  $\gamma_L^2 = 1$ . If  $\gamma_L^2 < 0$ , then one should try  $\langle L_3 \rangle_e = \langle \bar{e}_3 \rangle = \gamma_L x$  and  $\langle L_3 \rangle_\nu = 0$ . D-flatness now implies  $1 - \alpha^2 + \gamma_L^2 = 0$ . This also changes  $m_\ell^2 = m_{L_3}^2 + m_{\bar{e}_3}^2$ . In this case the top mass is  $M_t = y_t x$ , and the stop mass matrix entries are

$$\tilde{M}_{LL}^2 = m_{Q_3}^2 + y_t^2 x^2 + y_b^2 d^2 + \left( \frac{1}{12}g'^2 + \frac{1}{4}g_2^2 \right) d^2 , \quad (\text{A.25})$$

$$\tilde{M}_{RR}^2 = m_{\bar{u}_3}^2 + y_t^2 x^2 + y_t^2 d^2 - \frac{1}{3}g'^2 d^2 , \quad (\text{A.26})$$

$$\tilde{M}_{LR}^2 = -A_t y_t x . \quad (\text{A.27})$$

• **CCB(b)-UP:** In the CCB(b) case for the up-trilinear, the shifted fields are

$$\begin{aligned} \langle \Phi_u \rangle &= x , \\ \langle \Phi_d \rangle &= \gamma x , \\ \langle Q_1 \rangle_u &= \alpha x , \\ \langle \bar{u}_1 \rangle &= \beta x , \\ \langle L_3 \rangle_\nu &= \gamma_L x . \end{aligned} \quad (\text{A.28})$$

Unlike the previous CCB case ( $\gamma = 0$ ), this case has three terms whose phases ( $c_i = \cos \varphi_i$ ) are undetermined

$$2|A_u y_u \bar{u}_1 \Phi_u Q_1| c_1 + 2|\mu y_u \bar{u}_1 \Phi_d^\dagger Q_1| c_2 + 2|\mu B \Phi_u \Phi_d| c_3 . \quad (\text{A.29})$$

Reference [9] shows that this ambiguity can be resolved into two distinct possibilities. If  $\text{sign}(A_u) = -\text{sign}(B)$ , the three terms can be made simultaneously negative. If  $\text{sign}(A_u) = \text{sign}(B)$ , then the term of smallest magnitude is taken positive and the other two can be taken negative.

SU(3) D-flatness implies  $\beta^2 = \alpha^2$ . Also, U(1) and SU(2) D-flatness imply  $1 - \alpha^2 - \gamma^2 - \gamma_L^2 = 0$ . Consequently, the scalar potential appears as

$$V = y_u^2 \left( 2 + \alpha^2 \right) \alpha^2 x^4 + 2 \left( c_1 T_1 \alpha^2 + c_2 T_2 \alpha^2 |\gamma| + c_3 T_3 |\gamma| \right) x^2 + \left[ M^2 \alpha^2 + (m_1^2 - m_\ell^2) \gamma^2 + m_2^2 + m_\ell^2 \right] x^2 , \quad (\text{A.30})$$

where

$$T_1 = |A_u y_u x| , \quad (\text{A.31})$$

$$T_2 = |y_u \mu x| , \quad (\text{A.32})$$

$$T_3 = |\mu B| , \quad (\text{A.33})$$

$$M^2 = m_{Q_3}^2 + m_{\bar{u}_3}^2 - m_\ell^2 , \quad (\text{A.34})$$

$$m_1^2 = m_{\Phi_d}^2 + \mu^2 , \quad (\text{A.35})$$

$$m_2^2 = m_{\Phi_u}^2 + \mu^2 , \quad (\text{A.36})$$

$$(\text{A.37})$$

and where  $m_\ell^2 = m_{L_3}^2$  and  $c_i = \cos \varphi_i$ . Minimization with respect to  $\alpha^2$  and  $|\gamma|$  (note that the potential is a function of  $|\gamma|$ ) yields

$$|\gamma| = \frac{c_2 T_2 \alpha^2 + c_3 T_3}{m_\ell^2 - m_1^2} , \quad (\text{A.38})$$

$$\alpha^2 = -\frac{y_u^2 x^2 + M^2/2 + c_1 T_1 + c_2 T_2 |\gamma|}{y_u^2 x^2} . \quad (\text{A.39})$$

It must be confirmed that both  $\alpha^2 > 0$  and  $|\gamma| > 0$ . Otherwise these are set to zero. It must also be checked that  $\gamma_L^2 > 0$ . Otherwise one should try  $\langle L_3 \rangle_e = \langle \bar{e}_3 \rangle = \gamma_L x$  and  $\langle L_3 \rangle_\nu = 0$ . D-flatness now implies  $1 - \alpha^2 - \gamma^2 + \gamma_L^2 = 0$ . This also changes  $m_\ell^2 = m_{L_3}^2 + m_{\bar{e}_3}^2$ . In this case the top mass is  $M_t = y_t x$ , and the stop mass matrix entries are

$$\tilde{M}_{LL}^2 = m_{Q_3}^2 + y_t^2 x^2 , \quad (\text{A.40})$$

$$\tilde{M}_{RR}^2 = m_{\bar{u}_3}^2 + y_t^2 x^2 , \quad (\text{A.41})$$

$$\tilde{M}_{LR}^2 = y_t (\mu \gamma - A_t) x . \quad (\text{A.42})$$

• **CCB(b)-TOP:** In the CCB(b) case for the top-trilinear (there is no (a) case), the shifted fields are

$$\begin{aligned} \langle \Phi_u \rangle &= x , \\ \langle \Phi_d \rangle &= \gamma x , \\ \langle Q_3 \rangle_u &= \alpha x , \\ \langle \bar{u}_3 \rangle &= \beta x , \\ \langle L_3 \rangle_\nu &= \gamma_L x . \end{aligned} \quad (\text{A.43})$$

SU(3) D-flatness implies  $\beta^2 = \alpha^2$ . There is no imposition of D-flatness in the U(1) and SU(2) sectors. The potential now appears as

$$V = y_t^2 (2 + \alpha^2) \alpha^2 x^4 + [\alpha^2(m_{Q_3}^2 + m_{u_3}^2) + \gamma^2 m_1^2 + \gamma_L^2 m_{L_3}^2 + m_2^2] x^2 + 2 (c_1 T_1 \alpha^2 + c_2 T_2 \alpha^2 |\gamma| + c_3 T_3 |\gamma|) x^2 + \frac{1}{4} \hat{g}^2 (1 - \alpha^2 - \gamma^2 - \gamma_L^2) x^4, \quad (\text{A.44})$$

where

$$T_1 = |A_t y_t x|, \quad (\text{A.45})$$

$$T_2 = |y_t \mu x|, \quad (\text{A.46})$$

$$T_3 = |\mu B|, \quad (\text{A.47})$$

$$M^2 = m_{Q_3}^2 + m_{u_3}^2 - m_{L_3}^2, \quad (\text{A.48})$$

$$m_1^2 = m_{\Phi_d}^2 + \mu^2, \quad (\text{A.49})$$

$$m_2^2 = m_{\Phi_u}^2 + \mu^2. \quad (\text{A.50})$$

Minimization with respect to  $\gamma_L^2$  yields

$$\gamma_L^2 = 1 - \alpha^2 - \gamma^2 - \frac{2m_{L_3}^2}{\hat{g}^2 x^2}. \quad (\text{A.51})$$

If  $\gamma_L^2 > 0$ , then minimization with respect to  $\alpha^2$  and  $|\gamma|$  gives

$$|\gamma| = \frac{c_2 T_2 \alpha^2 + c_3 T_3}{m_{L_3}^2 - m_1^2}, \quad (\text{A.52})$$

$$\alpha^2 = -\frac{y_t^2 x^2 + M^2/2 + c_1 T_1 + c_2 T_2 |\gamma|}{y_t^2 x^2}. \quad (\text{A.53})$$

If  $\gamma_L^2 < 0$ , then it must be set to zero, and minimization with respect to  $\alpha^2$  and  $|\gamma|$  yields

$$2y_t^2 x^4 (1 + \alpha^2) - \frac{1}{2} \hat{g}^2 x^4 (1 - \alpha^2 - \gamma^2) + (m_{Q_3}^2 + m_{u_3}^2) x^2 + 2(c_1 T_1 + c_2 T_2 |\gamma|) x^2 = 0 \quad (\text{A.54})$$

$$-\hat{g}^2 x^4 (1 - \alpha^2 - \gamma^2) |\gamma| + 2|\gamma| x^2 m_1^2 + 2(c_2 T_2 \alpha^2 + c_3 T_3) x^2 = 0. \quad (\text{A.55})$$

Substituting for  $|\gamma|$  yields a cubic equation for  $\alpha^2$ . It must still be checked that both  $|\gamma| > 0$  and  $\alpha^2 > 0$ . In this case the top mass is  $M_t = y_t x$ , and the stop mass matrix entries are

$$\begin{aligned} \tilde{M}_{LL}^2 &= m_{Q_3}^2 + y_t^2 x^2 (1 + \alpha^2) + \frac{1}{12} g'^2 \left[ 1 - \frac{2}{3} \alpha^2 - \gamma^2 - \gamma_L^2 \right] x^2 \\ &\quad - \frac{1}{4} g_2^2 \left[ 1 - 3\alpha^2 - \gamma^2 - \gamma_L^2 \right] x^2 + \frac{1}{3} g_3^2 \left[ \alpha^2 x^2 \right], \end{aligned} \quad (\text{A.56})$$

$$\tilde{M}_{RR}^2 = m_{u_3}^2 + y_t^2 x^2 (1 + \alpha^2) - \frac{1}{3} g'^2 \left[ 1 - \frac{7}{3} \alpha^2 - \gamma^2 - \gamma_L^2 \right] x^2 + \frac{1}{3} g_3^2 \left[ \alpha^2 x^2 \right], \quad (\text{A.57})$$

$$\tilde{M}_{LR}^2 = y_t (\mu \gamma - A_t) x + \left[ y_t^2 - \frac{1}{3} \left( \frac{1}{3} g'^2 + g_3^2 \right) \right] x^2 \alpha \beta. \quad (\text{A.58})$$

• **CCB(a)-ELECTRON:** In the CCB(a) case for the electron-trilinear, the shifted fields are

$$\begin{aligned}
\langle \Phi_d \rangle &= x , \\
\langle \Phi_u \rangle &= 0 , \\
\langle L_1 \rangle_e &= \alpha x , \\
\langle \bar{e}_1 \rangle &= \beta x , \\
\langle Q_3 \rangle_u^2 &= \langle \bar{u}_3 \rangle^2 = u^2 = \left| \frac{\mu x}{y_t} \right| .
\end{aligned} \tag{A.59}$$

D-flatness implies  $\alpha^2 = \beta^2$  and  $\alpha^2 x^2 = x^2 + u^2$ . The scalar potential appears as

$$V = y_e^2 (2 + \alpha^2) \alpha^2 x^4 + [m_{\Phi_d}^2 + \alpha^2(m_{L_1}^2 + m_{\bar{e}_1}^2)] x^2 + (m_{Q_3}^2 + m_{\bar{u}_3}^2) u^2 - 2T_1 \alpha^2 x^2 , \tag{A.60}$$

where  $T_1 = |A_e y_e x|$ . In this case we use the bottom/sbottom contribution. The bottom mass is  $M_b = y_b x$ , and the sbottom mass matrix entries are

$$\tilde{M}_{LL}^2 = m_{Q_3}^2 + y_b^2 x^2 + \left( y_t^2 + \frac{1}{2} g_2^2 \right) u^2 , \tag{A.61}$$

$$\tilde{M}_{RR}^2 = m_{\bar{d}_3}^2 + y_b^2 (x^2 + u^2) , \tag{A.62}$$

$$\tilde{M}_{LR}^2 = A_b y_b x . \tag{A.63}$$

• **CCB(b)-ELECTRON:** In the CCB(b) case for the electron-trilinear, the shifted fields are

$$\begin{aligned}
\langle \Phi_d \rangle &= x , \\
\langle \Phi_u \rangle &= \gamma x , \\
\langle L_1 \rangle_e &= \alpha x , \\
\langle \bar{e}_1 \rangle &= \beta x .
\end{aligned} \tag{A.64}$$

D-flatness again implies  $\beta^2 = \alpha^2$  and  $\alpha^2 = 1 - \gamma^2$ . The potential appears as

$$\begin{aligned}
V = y_e^2 (2 + \alpha^2) \alpha^2 x^4 + [m_1^2 + \gamma^2 m_2^2 + \alpha^2(m_{L_1}^2 + m_{\bar{e}_1}^2)] x^2 \\
+ 2(c_1 T_1 \alpha^2 + c_2 T_2 \alpha^2 |\gamma| + c_3 T_3 |\gamma|) x^2 ,
\end{aligned} \tag{A.65}$$

where

$$T_1 = |A_e y_e x| , \tag{A.66}$$

$$T_2 = |y_e \mu x| , \tag{A.67}$$

$$T_3 = |\mu B| . \tag{A.68}$$

Substituting for  $\alpha^2$  and minimizing with respect to  $|\gamma|$  gives the following cubic equation

$$|\gamma|^3 [2y_e^2 x^2] - \gamma^2 [3c_2 T_2] + |\gamma| [(m_2^2 - m_{L_1}^2 - m_{\bar{e}_1}^2) - 4y_e^2 x^2 - 2c_1 T_1] + [c_2 T_2 + c_3 T_3] = 0 . \tag{A.69}$$

It must be checked that both  $|\gamma| > 0$  and  $\alpha^2 > 0$ . In this case the top mass is  $M_t = \gamma y_t x$ , and the stop mass matrix entries are

$$\tilde{M}_{LL}^2 = m_{Q_3}^2 + \gamma^2 y_t^2 x^2 , \quad (\text{A.70})$$

$$\tilde{M}_{RR}^2 = m_{u_3}^2 + \gamma^2 y_t^2 x^2 , \quad (\text{A.71})$$

$$\tilde{M}_{LR}^2 = y_t (\mu - \gamma A_t) x . \quad (\text{A.72})$$

If  $\gamma = 0$ , then we use the bottom/sbottom contribution. The bottom mass is  $M_b = y_b x$ , and the sbottom mass matrix entries are

$$\tilde{M}_{LL}^2 = m_{Q_3}^2 + y_b^2 x^2 , \quad (\text{A.73})$$

$$\tilde{M}_{RR}^2 = m_{d_3}^2 + y_b^2 x^2 , \quad (\text{A.74})$$

$$\tilde{M}_{LR}^2 = A_b y_b x . \quad (\text{A.75})$$

## APPENDIX B:

We find that Eq. (2.3) cannot be reliably calculated using our computer for large ( $> 10^6$ ) values of the VEVs. We therefore use a limiting form of this expression in the large VEV limit. This limiting form of  $\Delta V_1$  is presented in this appendix. We begin with some definitions:

$$m_t = y_t x \tag{B.1}$$

$$M_{LL}^2 = m_t^2 + m_L^2 + M_L x + G_L x^2 \tag{B.2}$$

$$M_{RR}^2 = m_t^2 + m_R^2 + M_R x + G_R x^2 \tag{B.3}$$

$$M_{LR}^2 = M x + G x^2 . \tag{B.4}$$

These expressions cover all the cases we have analyzed, and it is a simple matter to identify the various coefficients for each case. Note that in the CCB-ELECTRON cases,  $m_t$  should be substituted with  $m_b$ . In terms of these definitions, the two stop masses are

$$M_{i\pm}^2 = \frac{1}{2} \left[ 2m_t^2 + (m_L^2 + m_R^2) + (M_L + M_R)x + (G_L + G_R)x^2 \right] \pm \left\{ \left[ (m_L^2 - m_R^2) + (M_L - M_R)x + (G_L - G_R)x^2 \right]^2 + 4 \left[ Mx + Gx^2 \right]^2 \right\}^{1/2} . \tag{B.5}$$

To simplify the notation some new definitions are used, and the stop masses rewritten in terms of these

$$M_{i\pm}^2 = m_t^2 \left[ 1 + \left( \frac{G_{\pm}}{2y_t^2} \right) + \frac{1}{m_t} \left( \frac{M_{\pm}}{2y_t} \right) + \frac{1}{m_t^2} \left( \frac{m_{\pm}^2}{2} \right) \right] \pm \frac{1}{2} m_t^2 \left[ \alpha^2 + \frac{1}{m_t} \beta^2 + \frac{1}{m_t^2} \gamma^2 + \frac{1}{m_t^3} \delta^2 + \frac{1}{m_t^4} \epsilon^2 \right]^{1/2} \tag{B.6}$$

where

$$G_{\pm} = G_L \pm G_R \tag{B.7}$$

$$M_{\pm} = M_L \pm M_R \tag{B.8}$$

$$m_{\pm}^2 = m_L^2 \pm m_R^2 \tag{B.9}$$

$$\alpha^2 = (G_-^2 + 4G^2)/y_t^4 \tag{B.10}$$

$$\beta^2 = 2(G_- M_- + 4MG)/y_t^3 \tag{B.11}$$

$$\gamma^2 = (M_-^2 + 2m_-^2 G_- + 4M^2)/y_t^2 \tag{B.12}$$

$$\delta^2 = 2m_-^2 M_- / y_t \tag{B.13}$$

$$\epsilon^2 = m_-^4 . \tag{B.14}$$

Modulo overall factors the 1-loop correction is

$$\overline{\Delta V_1} = -2m_t^4 \ln\{m_t^2/\tilde{Q}^2\} + M_{t+}^4 \ln\{M_{t+}^2/\tilde{Q}^2\} + M_{t-}^4 \ln\{M_{t-}^2/\tilde{Q}^2\} \tag{B.15}$$

where  $\tilde{Q} = Qe^{3/4}$ . There are three cases to be considered

- case (a):  $\alpha^2 \neq 0$ ,

$$A_{\pm} = 1 + \frac{G_{\pm}}{2y_t} \pm \frac{\alpha}{2} \quad (\text{B.16})$$

$$B_{\pm} = \frac{M_{\pm}}{2y_t} \pm \frac{\beta^2}{4\alpha} \quad (\text{B.17})$$

$$C_{\pm} = \frac{m_{\pm}^2}{2} \pm \frac{4\alpha^2\gamma^2 - \beta^4}{16\alpha^3} \quad (\text{B.18})$$

- case (b):  $\alpha^2 = 0$  ( $\Rightarrow \beta^2 = 0$ );  $\gamma^2 \neq 0$ ,

$$A_{\pm} = 1 + \frac{G_{\pm}}{2y_t} \quad (\text{B.19})$$

$$B_{\pm} = \frac{M_{\pm}}{2y_t} \pm \frac{\gamma}{2} \quad (\text{B.20})$$

$$C_{\pm} = \frac{m_{\pm}^2}{2} \pm \frac{\delta^2}{4\gamma} \quad (\text{B.21})$$

- case (c):  $\alpha^2 = \beta^2 = \gamma^2 = \delta^2 = 0$ ;  $\epsilon^2 \neq 0$ ,

$$A_{\pm} = 1 + \frac{G_{\pm}}{2y_t} \quad (\text{B.22})$$

$$B_{\pm} = \frac{M_{\pm}}{2y_t} \quad (\text{B.23})$$

$$C_{\pm} = \frac{m_{\pm}^2}{2} \pm \frac{\epsilon}{2} \quad (\text{B.24})$$

Finally the form of the 1-loop correction in the large  $m_t$  limit is

$$\begin{aligned} \overline{\Delta V_1} &= m_t^4 \left\{ \left[ 2(a_+ + a_-) + (a_+^2 + a_-^2) \right] L + \left( A_+^2 \ln A_+ + A_-^2 \ln A_- \right) \right. \\ &\quad + \frac{2}{m_t} [A_+ B_+ (1/2 + L + \ln A_+) + A_- B_- (1/2 + L + \ln A_-)] \\ &\quad + \frac{1}{m_t^2} [B_+^2 (3/2 + L + \ln A_+) + B_-^2 (3/2 + L + \ln A_-)] \\ &\quad \left. + 2A_+ C_+ (1/2 + L + \ln A_+) + 2A_- C_- (1/2 + L + \ln A_-) \right\} \quad (\text{B.25}) \end{aligned}$$

where  $L = \ln\{m_t^2/\tilde{Q}^2\}$  and  $a_{\pm} = A_{\pm} - 1$ . To arrive at  $\Delta V_1$ , multiply the above expression by  $3/32\pi^2$ .

## REFERENCES

- [1] H. Haber, Lectures presented at TASI-92, University of Colorado, Boulder, (hep-ph/9306207); X. Tata, in *The Standard Model and Beyond*, p. 304, edited by J. E. Kim, World Scientific (1991).
- [2] A. Chamseddine, R. Arnowitt and P. Nath, Phys. Rev. Lett. **49**, 970 (1982); R. Barbieri, S. Ferrara and C. Savoy, Phys. Lett. **B119**, 343 (1982); L. Hall, J. Lykken and S. Weinberg, Phys. Rev. **D27**, 2359 (1983); P. Nath, R. Arnowitt and A. Chamseddine, Nucl. Phys. **B227**, 121 (1983).
- [3] L. Ibanez and G. Ross, Phys. Lett. **110B**, 215 (1982); K. Inoue, A. Kakuto, H. Komatsu and S. Takeshita, Progr. Theor. Phys. **68**, 927 (1982); L. Alvarez-Gaume, M. Claudson and M. Wise, Nucl. Phys. **B207**, 96 (1982); J. Ellis, D. Nanopoulos and K. Tamvakis, Phys. Lett. **B121**, 123 (1983).
- [4] H. Haber, in *Properties of SUSY Particles*, L. Cifarelli and V. Khoze, Editors, World Scientific (1993).
- [5] For a recent review, see G. Jungman, M. Kamionkowski and K. Griest, Phys. Rep. **267**, 195 (1996); see also J. Ellis, CERN-TH.7083/93 (1993).
- [6] H. Baer, C. H. Chen, R. Munroe, F. Paige and X. Tata, Phys. Rev. **D51**, 1046 (1995).
- [7] J. M. Frere, D. R. T. Jones and S. Raby, Nucl. Phys. **B222**, 11 (1983); L. Alvarez-Gaume, M. Claudson and M. Wise, Nucl. Phys. **B221**, 495 (1984); J. P. Derendinger and C. Savoy, Nucl. Phys. **B237**, 307 (1984); C. Kounnas, A. B. Lahanas, D. Nanopoulos and M. Quiros, Nucl. Phys. **B236**, 438 (1984); M. Claudson, L. Hall and I. Hinchliffe, Nucl. Phys. **B228**, 501 (1983); M. Drees, M. Glück and K. Grassie, Phys. Lett. **B157**, 164 (1985); J. Gunion, H. Haber and M. Sher, Nucl. Phys. **B306**, 1 (1988); H. Komatsu, Phys. Lett. **B215**, 323 (1988).
- [8] G. Gamberini, G. Ridolfi and F. Zwirner, Nucl. Phys. **B331**, 331 (1990).
- [9] J.A. Casas, A. Lleyda, and C. Muñoz, FTUAM-95-11 (Jun. 1995), hep-ph/9507294.
- [10] H. Baer and M. Brhlik, Phys. Rev. **D53**, 597 (1996).
- [11] G.W. Anderson and D.J. Castaño, Phys. Rev. **D53**, 2403 (1996).
- [12] H. Baer, M. Brhlik, R. Munroe and X. Tata, Phys. Rev. **D52**, 5031 (1995).
- [13] H. Baer, C. H. Chen, C. Kao and X. Tata, Phys. Rev. **D52**, 1565 (1995); H. Baer, C. H. Chen, F. Paige and X. Tata, FSU-HEP-960415 (1996), hep-ph/9604406.
- [14] H. Baer, C. H. Chen, F. Paige and X. Tata, Phys. Rev. **D52**, 2746 (1995) and Phys. Rev. **D53**, 6241 (1996).
- [15] T. Tsukamoto, K. Fujii, H. Murayama, M. Yamaguchi and Y. Okada, Phys. Rev. **D51**, 3153 (1995); H. Baer, R. Munroe and X. Tata, FSU-HEP-960601 (1996), hep-ph/9606325.
- [16] A. Kusenko, P. Langacker and G. Segre, UPR-0677-T (Feb. 1996), hep-ph/9602414.
- [17] A. Strumia, FTUAM-96-14 (Apr. 1996), hep-ph/9604417.
- [18] G. W. Anderson, private communication.
- [19] See, for example, M. Sher, Phys. Repts. **179**, 273 (1989).
- [20] B. de Carlos and J. A. Casas, Phys. Lett. **B309**, 320 (1993).
- [21] D. J. Castaño, E. J. Piard, and P. Ramond, Phys. Rev. **D49**, 4882 (1994).
- [22] V.S. Kaplunovsky and J. Louis, Phys. Lett. **B306**, 269 (1993).
- [23] A. Brignole, L.E. Ibañez, and C. Muñoz, Nuc. Phys. **B422**, 125 (1994).

## FIGURES

FIG. 1. Plots of the 1-loop correction, tree and 1-loop effective potentials along the MSSM and UFB-3(a) vacuum directions in the  $A_0 = 0$ ,  $m_0 = 100$  GeV,  $m_{1/2} = 200$  GeV,  $\mu < 0$ , and  $\tan \beta = 2$  case. Renormalization group improvement was implemented using the  $\alpha$ -prescription.

FIG. 2. Plots similar to Fig. 1 but with renormalization group improvement implemented using the  $\omega$ -prescription.

FIG. 3. Plots of the logarithm of the VEV versus  $\chi$ , a parameter appearing in the renormalization group improvement function, for the vacuum directions UFB-3(b) and CCB(a)-UP.

FIG. 4. Evolution of the VEV by using the renormalization group  $\gamma$  functions of the Higgs fields (solid line) and by tracking the minimum of 1-loop potential (dashed line) as a function of the renormalization scale  $Q$ .

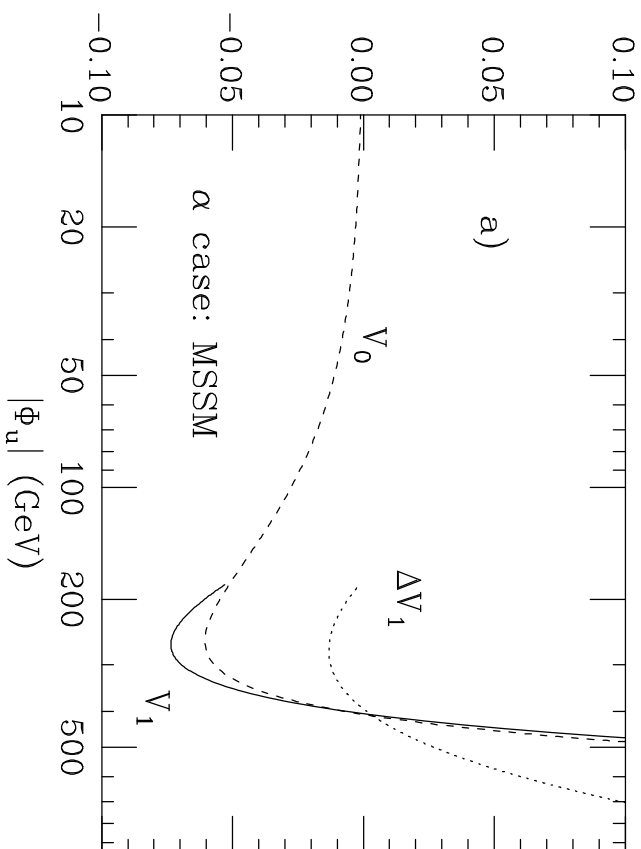
FIG. 5. Plots of the potential in the CCB(a)-UP case. In (a) the tree potential is displayed. In (b) the 1-loop potential is displayed for both  $\alpha$  and  $\omega$  prescriptions.

FIG. 6. Exclusion plots for the  $m_0$  vs.  $m_{1/2}$  plane based on the UFB-3(a) constraint. The squares represent  $2 < \eta < 3$ , the crosses  $3 < \eta < 4$ , and the x's  $4 < \eta < 5$ .

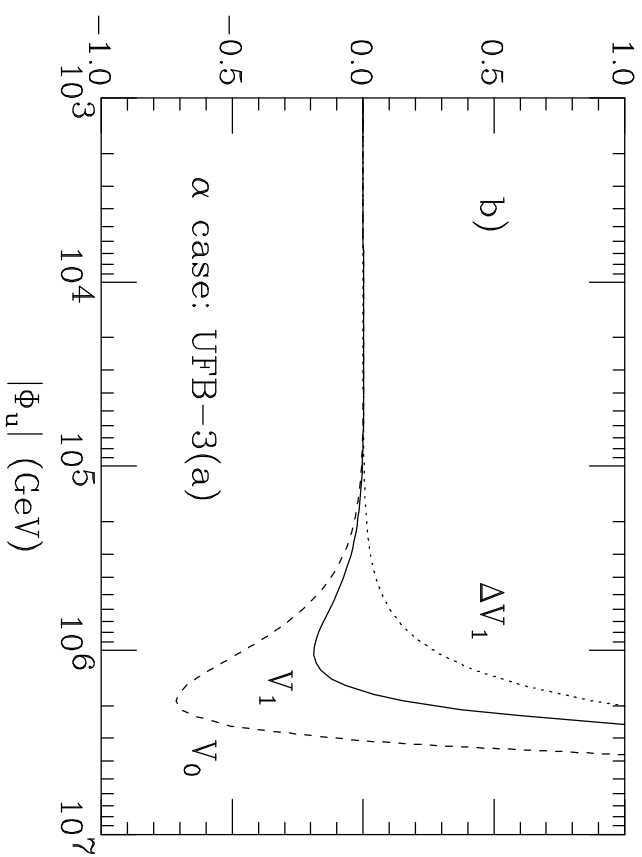
FIG. 7. Exclusion plots for the  $m_0$  vs.  $A_0$  plane based on the UFB-3(a) constraint and with  $m_{1/2} = 200$  GeV. The symbols are the same as in Fig. 6.

FIG. 8. Same as Fig. 6 but with superposed dark matter (dot dashes and solid) and naturalness (dashes) contours.

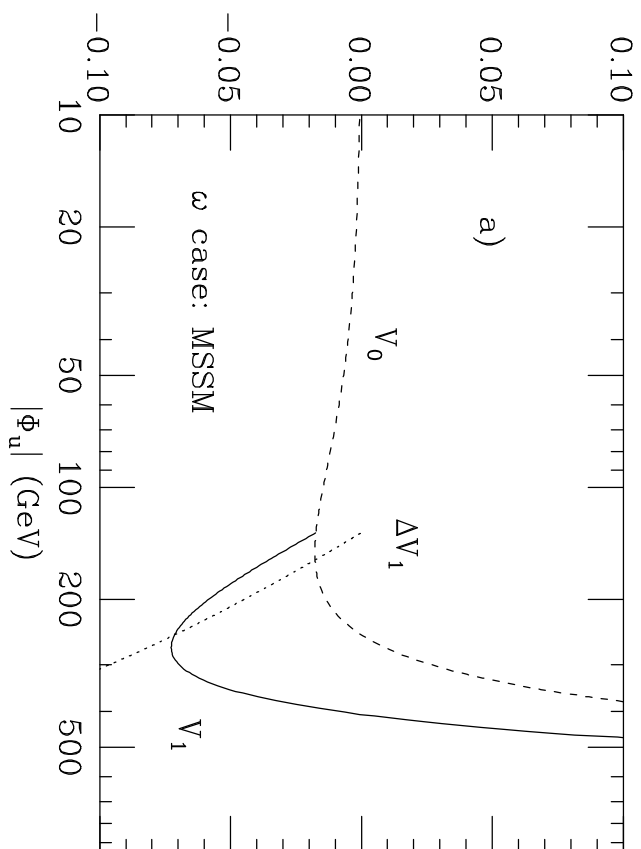
$V (10^{10} \text{ GeV}^4)$



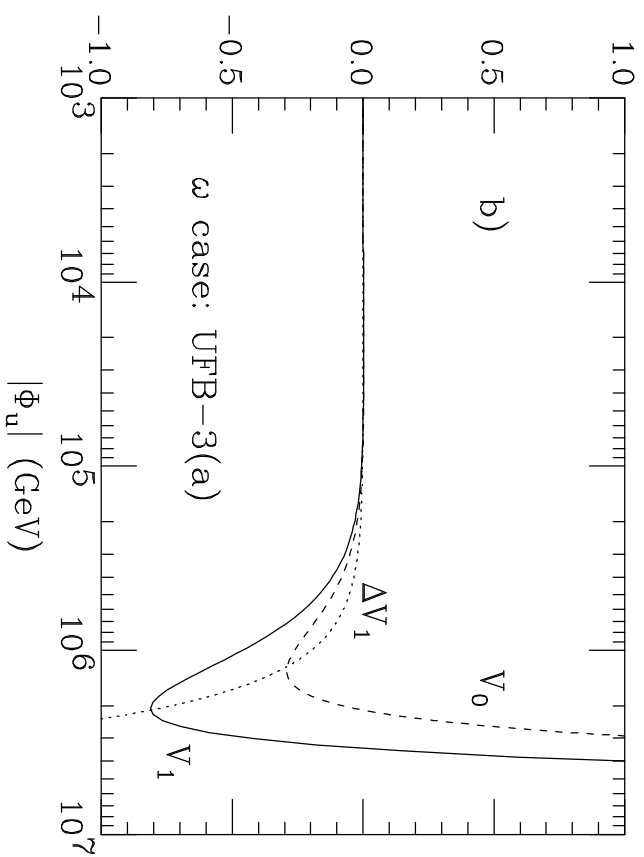
$V (10^{16} \text{ GeV}^4)$



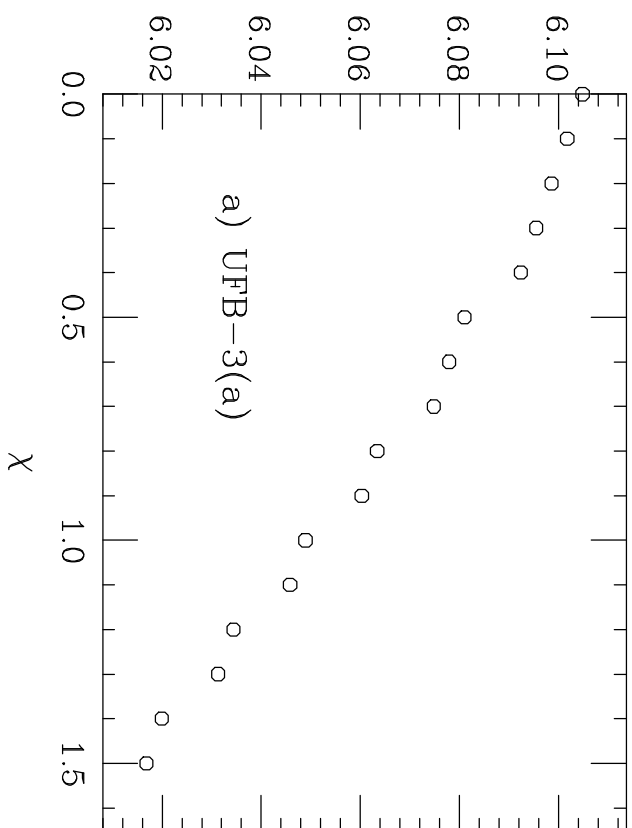
$V (10^{10} \text{ GeV}^4)$



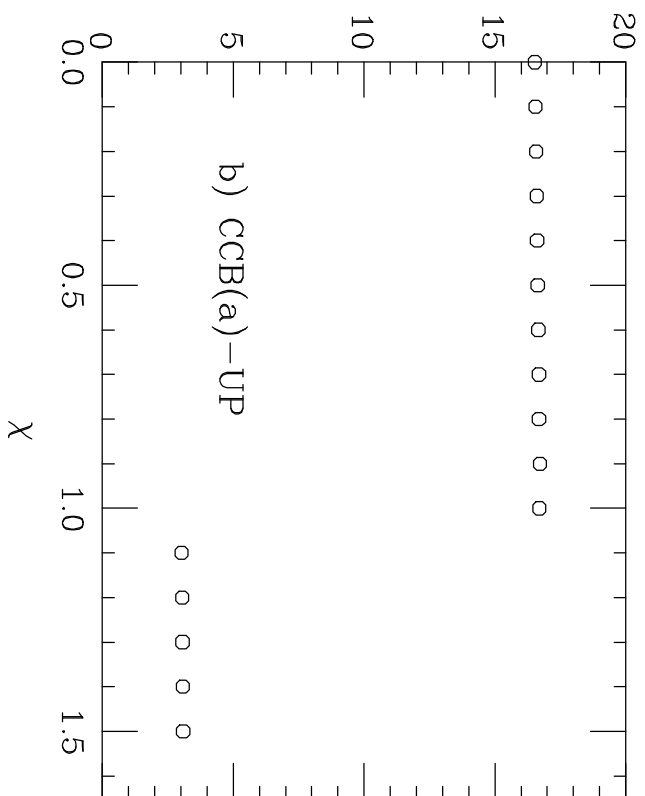
$V (10^{16} \text{ GeV}^4)$

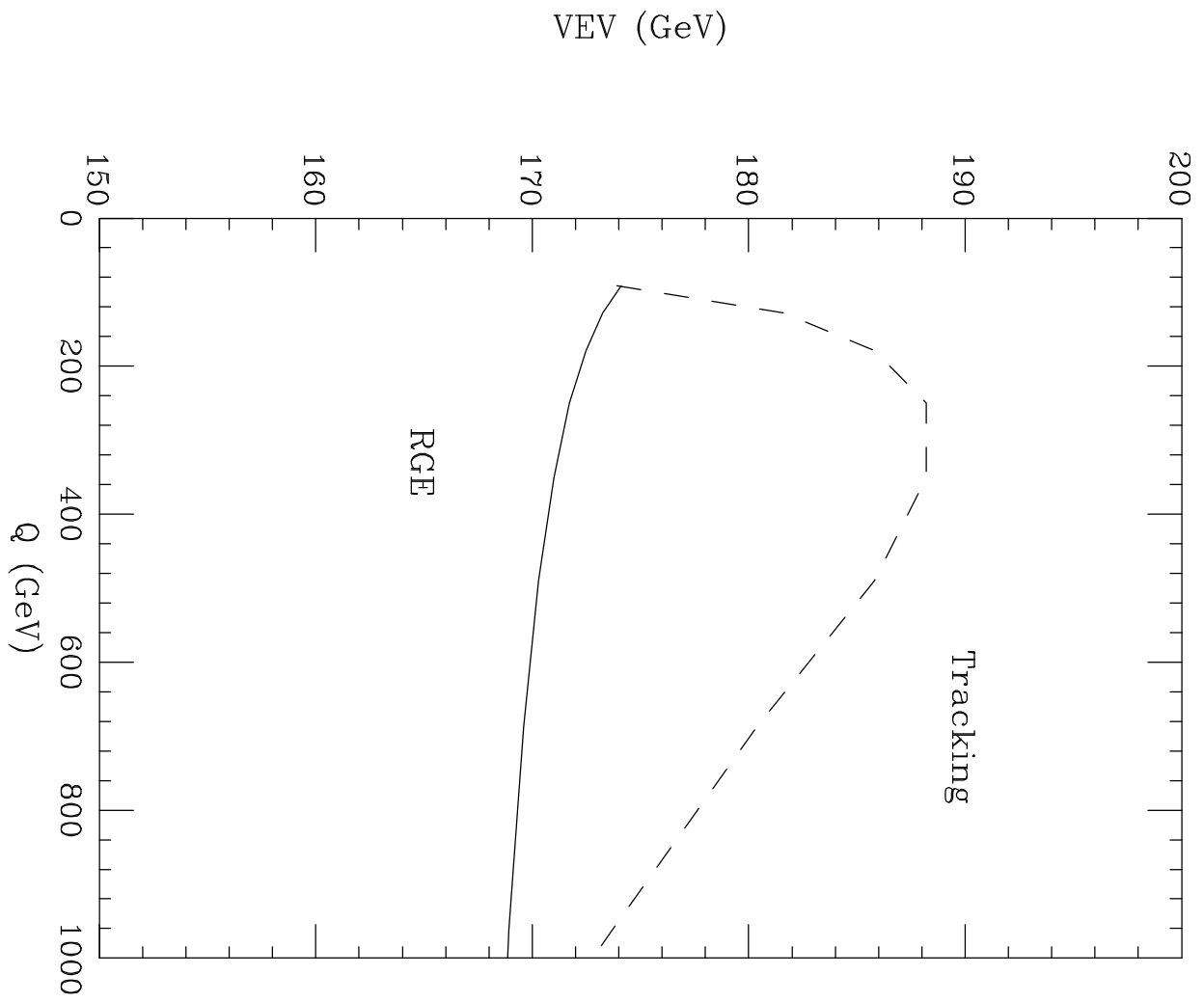


$\log_{10}(\text{vev})$

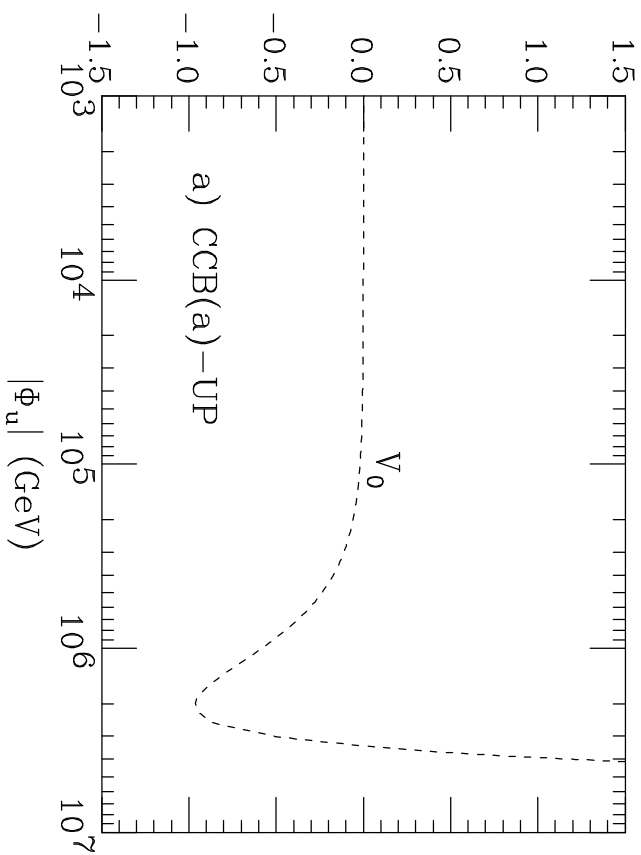


$\log_{10}(\text{vev})$





$V (10^{16} \text{ GeV}^4)$



$V (10^{50} \text{ GeV}^4)$

